10^{-11} year^{-1}) is less than the uncertainty in the J_2 rate given by (*5*), confirming that the climatic effects considered here account for the observed change in J_2 slope within the uncertainty of the observations.

In summary, our findings demonstrate that the J_2 slope reversal observed in 1997–98 (*5*) was the result of dramatic changes in oceanic and glacial mass distribution at that time. Our modeling results show that an equatorward mass shift in the oceans contributed a substantial portion of the J_2 increase during 1998 (Figs. 1B and 2B; figs. S1 and S2), coincident with phase reversals in both ENSO and the PDO. The year 1998 also saw the warmest global mean surface temperature on record (*25*), and we found that a concomitant surge in subpolar glacial melting (*13*, *26*) can account for nearly all of the remaining nonlinear behavior in the J_2 observations (Figs. 1C and 2C; Table 1). However, the dynamical links between these relatively rapid mass shifts and concurrent climate anomalies remain to be established. Further knowledge of Earth system processes, in particular polar ice sheet ablation (*27*), is needed to form a more comprehensive picture of ongoing mass balance changes and their climatic origins. New sources of geodetic data, such as the monthly time-variable gravity fields to be supplied by the recently launched GRACE mission (*28*), may soon revolutionize our ability to monitor and interpret these changes.

References and Notes

1. J. O. Dickey *et al.*, *Satellite Gravity and the Geosphere* (National Research Council, Washington, DC, 1997).
2. The definition and method of calculation for J_2 are given in the SOM Text.
3. C. F. Yoder *et al.*, *Nature* **307**, 757 (1983).
4. F. R. Stephenson, L. V. Morrison, *Philos. Trans. R. Soc. A* **351**, 165 (1995).
5. C. M. Cox, B. F. Chao, *Science* **297**, 831 (2002).
6. A. Cazenave, R. S. Nerem, *Science* **297**, 783 (2002).
7. S. R. Hare, N. J. Mantua, *Progr. Oceanogr.* **47**, 103 (2000).
8. T/P and XBT data were assimilated into the model run starting in 1993. Further details regarding the ECCO assimilation system are available at www.ecco-group.org. A brief summary is given in the SOM Text.
9. E. Rignot, R. H. Thomas, *Science* **297**, 1502 (2002).
10. M. B. Dyurgerov, M. F. Meier, *Arct. Alpine Res.* **29**, 379 (1997).
11. ———, *Arct. Alpine Res.* **29**, 392 (1997).
12. ———, *Proc. Natl. Acad. Sci. U.S.A.* **97**, 1406 (2000).
13. Annual volume changes in subpolar and mountain glaciers were obtained from the NSIDC Web site www-nsidc.colorado.edu/sotc/glacier_balance.html, courtesy of M. Dyurgerov, Institute of Arctic and Alpine Research, University of Colorado, Boulder.
14. T. S. James, E. R. Ivins, *J. Geophys. Res.* **102**, 605 (1997).
15. Glacial contributions to sea level change are not included in the ocean model, which is constrained to have constant volume (Boussinesq approximation). Before computing the oceanic J_2 contribution, the model bottom pressures are adjusted uniformly such that the global ocean mass is time-invariant.
16. E. M. Kalnay *et al.*, *Bull. Am. Meteorol. Soc.* **77**, 437 (1996).
17. The IB assumption accounts for oceanic compensation of atmospheric loading by substituting a spatially averaged uniform surface pressure field over the global ocean.
18. Because atmospheric pressure trends over Antarctica are poorly constrained due to a lack of data and calibration problems (*19*, *20*), we extended the IB assumption to include the land surface of Antarctica in this study.
19. K. M. Hines, D. H. Bromwich, G. J. Marshall, *J. Clim.* **13**, 3940 (2000).
20. G. J. Marshall, *J. Clim.* **15**, 659 (2002).
21. The model bottom pressure is directly proportional to the mass-per-unit area above a given point.
22. P. Johnston, K. Lambeck, *Geophys. J. Int.* **136**, 537 (1999).
23. R. Devoti *et al.*, *Geophys. Res. Lett.* **28**, 855 (2001).
24. R. Sabadini, B. L. A. Vermeersen, in *Ice Sheets, Sea Level and the Dynamic Earth*, vol. 29 of Geodynamics Series, J. X. Mitrovica, B. L. A. Vermeersen, Eds. (American Geophysical Union, Washington, DC, 2002).
25. J. Hansen *et al.*, *J. Geophys. Res.* **104**, 30,997 (1999).
26. J. Oerlemans, *Ann. Glaciol.* **31**, 44 (2000).
27. H. J. Zwally *et al.*, *Science* **297**, 218 (2002).
28. D. Adam, *Nature* **416**, 10 (2002)

29. The authors gratefully acknowledge discussions (both oral and via e-mail) with J.-P. Boy, D. Bromwich, B. F. Chao, Y. Chao, C. M. Cox, M. B. Dyurgerov, L.-L. Fu, M. Ghil, E. Ivins, K. Mo, and Y.Yung, and the constructive comments of the reviewers. The work of J.O.D., S.L.M., and I.F. presents the results of one phase of research carried out at the Jet Propulsion Laboratory, under contract with the National Aeronautics and Space Administration. O.D.V. is a postdoctoral researcher of the National Fund for Scientific Research, Belgium. This work was accomplished during O.D.V.'s visit to JPL during Summer 2002. This is a contribution of the ECCO consortium funded by the National Oceanographic Partnership Program.

Supporting Online Material

www.sciencemag.org/cgi/content/full/298/5600/1975/DC1
Materials and Methods
SOM Text
Figs. S1 and S2
Table S1
References and Notes

27 August 2002; 4 November 2002

Environmental Effects of Large Impacts on Mars

Teresa L. Segura,[1*†] Owen B. Toon,[1] Anthony Colaprete,[2] Kevin Zahnle[2]

The martian valley networks formed near the end of the period of heavy bombardment of the inner solar system, about 3.5 billion years ago. The largest impacts produced global blankets of very hot ejecta, ranging in thickness from meters to hundreds of meters. Our simulations indicated that the ejecta warmed the surface, keeping it above the freezing point of water for periods ranging from decades to millennia, depending on impactor size, and caused shallow subsurface or polar ice to evaporate or melt. Large impacts also injected steam into the atmosphere from the craters or from water innate to the impactors. From all sources, a typical 100-, 200-, or 250-kilometers asteroid injected about 2, 9, or 16 meters, respectively, of precipitable water into the atmosphere, which eventually rained out at a rate of about 2 meters per year. The rains from a large impact formed rivers and contributed to recharging aquifers.

The valley networks on Mars cut across the heavily cratered southern highlands, the oldest terrain on the planet, signifying that they are contemporaneous with the period of heavy cometary and asteroidal bombardment of Mars and of the rest of the inner solar system (*1*, *2*). There are about 25 visible craters with diameters between 600 and 4000 km (fig. S1) (*3*). Many other large craters may have been erased by resurfacing events (*4*). Here we consider how impacts might have caused water to flow on Mars and create the valley networks.

An asteroid (*5*) with a diameter of 100 (200, 250) km and traveling at 9 km/s delivers about 6×10^{25} (4×10^{26}, 9×10^{26}) J of energy to the planet and generates a crater ~600 (1000, 1300) km in diameter (fig. S1) and 3×10^{18} (3×10^{19}, 5×10^{19}) kg of ejecta (*6*–*8*) (Fig. 1). Ejecta include vaporized and melted impactor and target materials. About 20% of the ejecta are rock vapors (*6*); most of the rest is melt (*7*). Only a few percent of the ejecta mass would escape from Mars, given a 9 km/s impact velocity (*6*). In the case of large impacts, the ejecta are hot because of the large energy release and because of the low surface-to-volume ratio of the ejecta, which inhibits cooling. The hot ejecta are distributed globally both ballistically and via the thermally expanding vapor cloud. For a time, the rock vapor is suspended in the hot atmosphere because it is too warm to condense immediately.

There are several primary sources of water. The impactor itself may deliver water. A 100 (200, 250)-km asteroid that is 5% water by mass (*8*) would deliver 40 (310, 620) cm

[1]Program in Atmospheric and Oceanic Sciences, Laboratory for Atmospheric and Space Physics, University of Colorado, Campus Box 392, Boulder, CO 80309–0392, USA. [2]NASA-Ames Research Center, MS 245-3, Moffett Field, CA 94035, USA.

*Present address: NASA-Ames Research Center, MS 245-3, Moffett Field, CA 94035, USA.

†To whom correspondence should be addressed.

of water (global equivalent thickness). The crater is important if the deep regolith of Mars is wet, and as much as 100 (360, 540) cm of water could be liberated from the crater (*9*). Because the ejecta are hot, most of this water directly enters the atmosphere as vapor. A third possible source is vapor evaporated from exposed ice, such as the polar caps. If this ice were exposed, 30 (250, 500) cm of water would be liberated (*10*) (Fig. 1).

The suspended rock vapor eventually condenses and rains out into a global rock rain layer. The rain is hot (we estimate ~1600 K, but it might be as hot as 3000 K, depending on impactor size and surface pressure) because it did not completely radiatively cool. The water that was injected as a result of the vaporization of the impactor and target materials and as a result of the evaporation of the polar caps remains as vapor in the hot atmosphere.

We simulated the environment on Mars after the emplacement of the rock rain layer (*11*) and the injection of water into the atmosphere. We chose to model impacts of asteroids with diameters of 100, 200, and 250 km, using a one-dimensional (1D) radiative transfer code to calculate the evolution of the atmospheric temperature after the impact, coupled to a 1D model of the regolith to calculate the evolution of the surface temperature (*12*). The model was adjusted for early martian conditions by reducing the solar constant (the number of watts of incoming solar radiation per meter squared) from its present value (150.2 W/m^2) to 75% of its present value (112.6 W/m^2) and by increasing the post-impact CO_2 pressure from its present value of 7.1 mbar to 150 mbar (*13*). The model precipitates (*12*) all the water that was injected after the impact (Fig. 2). Once the water was rained out, it was considered lost from the system; we did not include a hydrological cycle in which the rainfall might evaporate back into the atmosphere, nor did we include the radiative properties of clouds, but their consideration in our model would only lengthen the warm periods reported here.

Below the fresh ejecta layer is the original martian regolith, which we assumed contains 20% water by mass under a 40-cm dry cap (*14*). Permafrost (up to 40% water) and substantial polar ice deposits (~95% water) may also be present (*15*). In addition, the soil might contain other materials, such as methane clathrates, that could liberate greenhouse gases that we ignored. We did not include the additional CO_2 that would come from melting the ice caps, which would likely occur because the surface temperatures reported here are well above the sublimation point for CO_2 at the assumed pressures. The additional greenhouse effect that would result from this CO_2 would only lengthen the warm period.

The regolith under the hot ejecta heats by thermal conduction; this thermal pulse melts water in the ground when the temperature is above 273 K (*12*) (Fig. 2). The subsurface water may evaporate into the atmosphere, which we have not considered. This would contribute additional greenhouse warming, prolonging the time above 273 K, and this water would eventually contribute to the rainfall totals. Our model also did not include convection in the regolith, which is relatively unimportant for the magnitude of events discussed here (*16*).

During the first few weeks after the impact of an asteroid 100 (200, 250) km in diameter, the modeled atmosphere warms from its assumed initial temperature, 500 K, until global surface temperatures reach 800 K (Fig. 3). Parts of the martian regolith may be kept above freezing for at least 2 years, 55 years, and 200 years by the 100-, 200-, and 250-km events, respectively (Fig. 3), and for millennia for even larger impacts (Fig. 4). The amount of water precipitated out of the atmosphere from vaporization of the impactor, target, and polar caps and melted below ground for asteroid impactors with different diameters yields global water totals ranging from 5 to 50 m for our examples, and up to 200 m for the largest objects (Fig. 4).

We envision two mechanisms for river formation. Because the ejecta are globally distributed, we do not expect that rivers should be located near the craters of the objects that created the rivers. The first mechanism is global rainout of the directly injected water from the cooling atmosphere. Average precipitation rates will exceed 2 m/year, depending on impactor size (Fig. 2). Flooding and mudslides will reshape the landscape, with eroded rivers containing high sediment loads as solids are broken apart by rushing water. The second mechanism is groundwater release during the long periods of time that the subsurface is above 273 K (Fig. 3). Heating from the hot ejecta will mobilize ground ice, and the precipitation will locally recharge these aquifers. It has been suggested (*17*) that most of the observed valleys were eroded by groundwater, but the absence of a recharge mechanism has frustrated this hypothesis. Impacts provide lengthy and abundant precipitation that may recharge the aquifers. Once rivers had been formed, substantial further erosion, guided by the river valleys, may have been caused by the wind (*18*).

It has been estimated (*19*) that a 50-m-deep

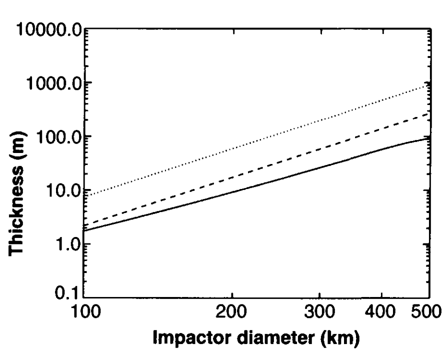

Fig. 1. The average ejecta layer thickness (dotted curve), global vaporized rock layer thickness (dashed curve), and global vaporized water thickness (solid curve) as a function of impactor diameter. The amount of debris that escapes to space has already been subtracted from these values. The slope of the water curve changes when the maximum polar water abundance (9) is reached (Fig. 4).

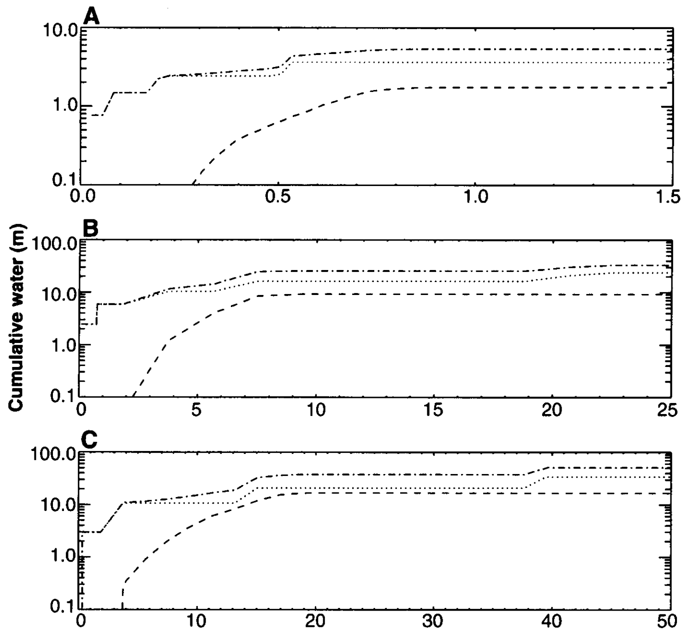

Fig. 2. Modeled atmospheric precipitation (dashed curves), subsurface melted water (dotted curves; a step function because of our subsurface model grid), and their sums (dash-dot curves) for the 100-km (**A**), 200-km (**B**), and 250-km (**C**) objects. The precipitation is zero until the atmosphere cools enough to condense water. Precipitation continues until all atmospheric water is exhausted, indicated by the maxima of the dashed curves.

global layer of water was needed to erode the valley networks. This is the equivalent of estimating the volume of debris that would have filled the valleys and the amount of water (assuming a water-to-rock ratio of 100:1) necessary to erode this valley fill away (*19*). We have shown that a single 250-km-diameter impact event, under our assumptions, may free 50 m of water. There are at least 12 visible craters on Mars, confirming the collisions of such objects (fig. S1B), and perhaps even more of these large basins are buried (*4*). Because the amount of water necessary for erosion of the valleys depends only on how much valley fill must be removed, it is irrelevant whether the water layer is the result of one impact or several. Thus the cumulative effects of smaller objects (<250 km) are also important. There may have been 100 million years between extreme events, but each impact event would have contributed to the ongoing erosion of the planet in the ways we have described. It is likely that over the long periods between impacts, the near-surface regolith would be recharged by very slow diffusion of water vapor into the subsoil (*20*), where it could be released again by the next large impact. When the impacts ceased, the erosion also ceased, and today we observe a planet with large craters and river valleys of approximately the same age. The rarity and brevity of the events we have described thwart the development of mature drainage systems, which are rare on Mars (*17*).

Data from the Pathfinder landing site indicate that erosion rates were 10^3 to 10^6 times higher about 3.5 to 4.5 billion years ago than the current rate of ~1 nm/year (*21*). These ancient erosion rates suggest the presence of an erosional agent that was active in the past, and the most likely candidate is water. However, for Mars to keep any liquid water on its surface requires higher surface temperatures than today. The CO_2 greenhouse models call for 1 to 5 bar of CO_2 for surficial liquid water, depending on the solar luminosity (*22*). At the solar luminosity expected early in the history of Mars, 5 bar of CO_2 may not be sufficient even when CO_2 clouds are considered (*23, 24*). The release of water and CO_2 is possible after volcanic events such as the building of Tharsis (*25*). However, the addition of 1 to 2 bar of CO_2 from this volcanic activity is not sufficient to bring the surface temperature above 273 K (*26*), so although a 120-m global H_2O layer is possible with this mechanism, the layer would probably be ice, rather than liquid water. Furthermore, with such large amounts of CO_2 in the atmosphere, along with liquid water on the surface, we would expect carbonates and clays to form, yet there is little or no evidence for carbonates or clays (*27*). Above, we demonstrated that meters of water may precipitate out and flow on Mars because of the effects of large asteroidal impacts, but do so during a period of time too brief to allow the formation of these minerals.

Another observable feature of repeated collisions of large objects should be the multiple ejecta blankets they may have emplaced. Figure 1 illustrates the thickness of debris blankets expected for impactors of a range of sizes. Although these layers may have been eroded during the early history of Mars, remnants of them may have been observed by the Mars Global Surveyor (*28*). Numerous debris layers have been identified that are contemporaneous with and intermixed with the valley networks and that apparently have a subaerial mode of deposition. These layers are precisely what would be expected from impacts that are large enough in size to generate the valleys through the mechanism we propose (*29*). Hence, a test of our hypothesis would entail careful comparisons between the ages of thick ejecta blankets and the initial formation times of the rivers.

Hypotheses of a warm, wet Mars, based on the presumption that the valley networks formed in a long-lasting greenhouse climate, imply that Mars may once have been teeming with life. In contrast, we envision a cold and dry planet, an almost endless winter broken by episodes of scalding rains followed by flash floods. Only during the brief years or decades after the impact events would Mars have been temperate, and only then might it have bloomed with life as we know it. We find that temperatures in the regolith after a large impact do not exceed the terrestrial boiling point (373 K) except in the topmost tens of meters or so of soil, providing a possible refuge for life deeper in the regolith. However, the short duration of the warm episodes predicted here may have made it challenging for life to establish itself on Mars in the first place.

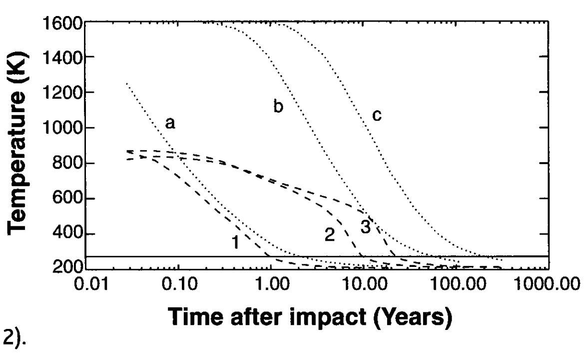

Fig. 3. Surface temperature (dashed curves) and maximum subsurface temperature (dotted curves) as a function of time, with the freezing point of water (solid) indicated for the 100-km (1 and a), 200-km (2 and b), and 250-km (3 and c) objects. The atmosphere cools more slowly with the larger objects, owing to the larger amount of water injected. The surface temperature decreases rapidly when the atmospheric water is exhausted (Fig. 2).

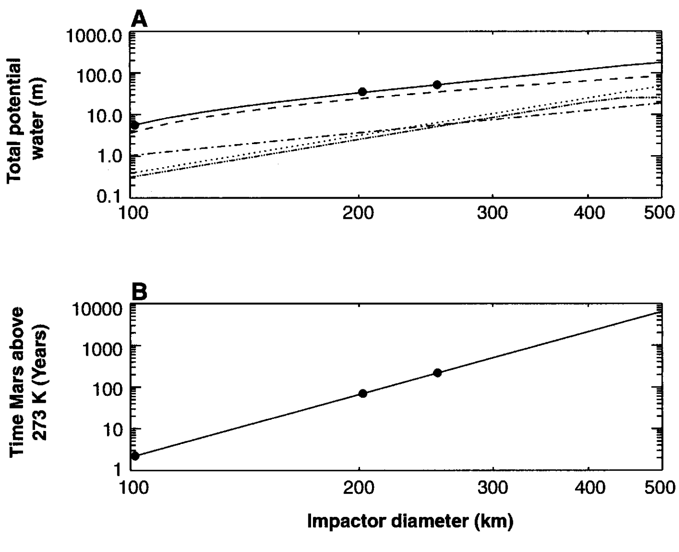

Fig. 4. (**A**) Amount of water from vaporization of the impactor (dotted curve), target material (dash–one dot curve), and polar caps (dash–two dot curve) (*9*), from melting the subsurface (dashed curve) and the total (solid curve) as a function of impactor size. (**B**) Time that the planet's regolith is above 273 K as a function of impactor size. The melted subsurface water amounts and time periods required for the regolith to be above 273 K are shown as data points for 100-, 200-, and 250-km objects. The curves are linear fits (water) and exponential fits (time periods) to the points, which are extended to larger sizes.

References and Notes

1. W. K. Hartmann *et al.*, in *Origin of the Earth and Moon*, R. M. Canup, K. Righter, Eds. (Univ. of Arizona Press, Tucson, AZ, 2000), pp. 493–512. These models indicate that the heavy bombardment period lasted from about 3.8 to 4.3 billion years ago.
2. B. A. Cohen, T. Swindle, D. Kring, *Science* **290**, 1754 (2000) and references therein. Studies of impact ages reveal that the late bombardment, whatever its duration, was felt through the inner solar system, Mars included.
3. K. L. Tanaka, D. Scott, R. Greeley, in *Mars*, H. H. Kieffer, B. Jakosky, C. Snyder, M. Matthews, Eds. (Univ. of Arizona Press, Tucson, AZ, 1992), pp. 345–382.
4. H. V. Frey, J. Roark, K. Shockey, E. Frey, S. Sakimoto, *Geophys. Res. Lett.* **29**, 10.1029/2001GL013832 (2002).
5. In addition to asteroids, comets may have struck Mars. If such a comet traveled faster than 15 km/s,

the debris from the comet itself would have been lost to space after the impact, because most of its vapor plume would have been hot enough to expand at speeds exceeding the escape velocity. For example, to excavate the same-sized crater as the asteroid 100 km in diameter, a comet would need to have a 110-km diameter and travel at 15 km/s, using the equation and assumptions discussed in (6), with density $\rho = 1$ g/cm^3. Such an object would produce a total (pulverized + global rock rain) ejecta layer of about 8 m. This is about as thick as the layer for an asteroid (Fig. 1) because most of it originates from the target material.
6. N. H. Sleep, K. Zahnle, *J. Geophys. Res.* **103**, 28529 (1998). We used equation 1 from Sleep and Zahnle and equations 9, 10, 13, and 18 from (*11*) to calculate the volume of debris, from the impactor and target, that escapes, vaporizes, and/or is globally distributed, using 1.4×10^7 J/kg and 6×10^6 J/kg for Qv (energy for complete vaporization) and Qv* (energy for incipient vaporization), respectively. These calculations are velocity-dependent; we have chosen an impacting velocity of 9 km/s.
7. E. Pierazzo, A. Vickery, H. Melosh, *Icarus* **127**, 408 (1997).
8. K. Lodders, B. Fegley Jr., *The Planetary Scientist's Companion* (Oxford Univ. Press, New York, 1998). Types CM and CI carbonaceous chondrites contain 12 to 18% water, respectively.
9. We estimate that the large crater excavates $W_{crater} = 0.25\, \pi\, \phi\, D_{crater}{}^2\, H$, where we take the porosity of the regolith to decrease exponentially with depth with a scale height, H, of 2.8 km (*29*), and where the porosity at the top of the regolith, ϕ, is 0.2 and the regolith pore space is filled with water.
10. If we presume that thermal radiation from the rock vapor radiates equally up and down, each precipitable centimeter of rock vapor evaporates $\rho_r\, L_{rock}/(2\, \rho_i\, L_{ice}) = 8$ cm of ice (where ρ_r is the density of rock and ρ_i is the density of ice) as the vapor condenses to form molten rock, where $L_{rock} = 1.4 \times 10^{11}$ erg/g is a characteristic latent heat of vaporization for rock. The current martian ice caps cover 1.7% of the planet to an average depth of 1.5 to 2 km (*30*).
11. K. Zahnle, *Spec. Pap. Geol. Soc. Am.* **247**, 271 (1990).
12. We use the correlated-*k* method to calculate the optical depths for CO_2 and H_2O and a two-stream radiative transfer model to calculate heating rates at each atmospheric level. Eddy diffusion handles vertical transport of static energy, which is used to update temperature and pressure at each level. Surface pressure of CO_2 is assumed to be 150 mbar (*13*). Relative humidity at each level is calculated and as the injected water condenses and rains out, we replace it with a radiatively inert gas to maintain hydrostatic equilibrium. The 30-layer subsurface model solves explicitly for temperature using the diffusion equation. When the temperature in a layer exceeds 273 K, the water melted is calculated and tabulated until that layer is dry. Additional materials and methods are available as supporting material on *Science* Online.
13. D. A. Brain, B. M. Jakosky, *J. Geophys. Res.* **103**, 22689 (1998). Although CO_2 pressures of bars may have occurred on early Mars, Brain and Jakosky have argued that the pressure remaining near the end of heavy bombardment was in the range from 30 to 600 mbar, depending on sputtering and impact erosion. 150 mbar of carbon dioxide only warms Mars a few degrees above its temperature of thermal emission to space, which was about 198 K.
14. W. V. Boynton *et al.* [*Science* **297**, 81 (2002)] used data from the Gamma-Ray Spectrometer onboard the Mars Odyssey to estimate that the current middle- and high-latitude martian regolith may be as much as 35% (±15%) water by weight, with a 40-cm dry (1% water) cap. We have chosen the lower limit of 20% for our simulations, with a 40-cm (0% water) dry cap to represent global average conditions. We recognize that these numbers pull away from our otherwise conservative approach, because Boynton *et al.* found these numbers to be for the polar regions and not global. However, we note that a colder Noachian Mars probably had a much shallower equatorial ice depth than at present. It is possible that local conditions were much dryer or wetter than these conditions. Runs of our model with a dry (1%) regolith confirm that the water evaporated from the target material and melted in the subsurface (Fig. 4) scales linearly with the water fraction. These two values dominate the curve, so if 1% water, for example, were more correct, the total water precipitated and melted would be 20 times less than our numbers, but there are still plenty of large events in the crater (visible and buried) record to generate the required water for valley formation.
15. M. C. Malin, *Geophys. Res. Lett.* **13**, 444 (1986).
16. Hydrothermal convection will occur in systems when the Rayleigh number, *Ra*, is greater than 40. The Rayleigh number is given by $Ra = \alpha\rho C_p g \lambda h \Delta T/(\eta k)$ (*31*) where α is the thermal expansion coefficient of water, g is gravity, ρ is the density of water, C_p is the specific heat of water, λ is the permeability of rock, h is the height over which the temperature differences occur, η is the viscosity of water, and k is the thermal conductivity of water. Our impact events have Rayleigh numbers of less than the threshold, so convection is not important. To fully estimate the importance of convection, we would need better information on the porosity of the martian regolith at depth, and so we have not included convection in our model. The most likely scenario for extensive groundwater flow would involve an impermeable capping layer, which would suppress such convection.
17. M. H. Carr, *Water on Mars* (Oxford Univ. Press, New York, 1996).
18. C. B. Leovy, J. C. Armstrong, in preparation.
19. M. H. Carr, M. C. Malin, *Icarus* **146**, 366 (2000).
20. B. M. Jakosky, *Icarus* **55**, 1 (1983).
21. M. P. Golombek, N. T. Bridges, *J. Geophys. Res. Planets* **105**, 1841 (2000).
22. J. B. Pollack, J. Kasting, S. Richardson, K. Poliakoff, *Icarus* **71**, 203 (1987).
23. F. Forget, R. T. Pierrehumbert, *Science* **278**, 1273 (1997).
24. A. Colaprete and O. B. Toon (*J. Geophys. Res.*, in press) found that only 5 to 10 K of warming was achieved when the radiative effects of CO_2 ice clouds were considered, which is not enough to heat the planet above 273 K.
25. R. J. Phillips *et al.*, *Science* **291**, 2587 (2001).
26. J. F. Kasting, *Icarus* **91**, 1 (1991).
27. P. R. Christiansen *et al.*, *Science* **279**, 1692 (1998).
28. M. C. Malin, K. S. Edgett, *Science* **290**, 1927 (2000).
29. The energy supplied by an impactor, added to the energy from the Sun, places Mars into the runaway greenhouse regime of several steady-state models. Given a sufficiently rapid supply of groundwater to the atmosphere, a temporary runaway might have begun. The magnitude of such an event is beyond the scope of this work to determine.
30. D. E. Smith *et al.*, *Science* **284**, 1495 (1999).
31. K. Zahnle, J. Pollack, J. Kasting, *Geochim. Cosmochim. Acta* **54**, 2577 (1990).
32. The authors thank the University of Colorado's Center for Astrobiology (grant NCC2-1052), the NASA Astrobiology Institute through Ames Research Center, and NASA (grant NAG5-6900) for support for this research.

Supporting Online Material
www.sciencemag.org/cgi/content/full/298/5600/1977/DC1
Materials and Methods
Fig. S1
References

3 May 2002; accepted 11 November 2002

Regulation of Oceanic Silicon and Carbon Preservation by Temperature Control on Bacteria

Kay D. Bidle,*† Maura Manganelli,‡ Farooq Azam

We demonstrated in laboratory experiments that temperature control of marine bacteria action on diatoms strongly influences the coupling of biogenic silica and organic carbon preservation. Low temperature intensified the selective regeneration of organic matter by marine bacteria as the silicon:carbon preservation ratio gradually increased from ~1 at 33°C to ~6 at −1.8°C. Temperature control of bacteria-mediated selective preservation of silicon versus carbon should help to interpret and model the variable coupling of silicon and carbon sinking fluxes and the spatial patterns of opal accumulation in oceanic systems with different temperature regimes.

Diatom productivity is largely responsible for downward fluxes of biogenic silica ($BSiO_2$; opal) and organic matter in the global ocean (*1, 2*). An understanding of the mechanisms that couple the relative fates of diatom Si and C within the water column is critical in order to elucidate the role of diatoms in the biological carbon pump and in order to use opal effectively for paleoproductivity reconstruction.

Oceanic systems display large regional differences in the accumulation and preservation of opal in sediments, but accumulation does not necessarily correspond to C and Si production rates (*3*). Only 25 to 40% of global biogenic silica production occurs above high-accumulation regions (regions consisting of >5% opal by weight), such as coastal upwelling zones, the subarctic Pacific, and the Southern Ocean (*3, 4*). The Southern Ocean alone supplies ~50% of the global opal accumulation, while accounting for only 20 to 30% of global opal production (*3–5*). In contrast, virtually no opal is ac-

Marine Biology Research Division, Scripps Institution of Oceanography, University of California San Diego, La Jolla, CA 92093–0202, USA.

*Present address: Institute of Marine and Coastal Science, Rutgers University, 71 Dudley Road, New Brunswick, NJ 08901–8521, USA.
†To whom correspondence should be addressed. E-mail: bidle@imcs.rutgers.edu
‡Present address: ISPESL–DIPIA, National Institute for Occupational Safety and Prevention, via Fontana Candida, 1, 00040 Monteporzio Catone (RM), Italy.